Redox Biology xxx (xxxx) xxxx

Contents lists available at ScienceDirect

Redox Biology

journal homepage: www.elsevier.com/locate/redox

Metabolic reprogramming of oncogene-addicted cancer cells to OXPHOS as a mechanism of drug resistance

Jayshree Hirpara[a,1], Jie Qing Eu[a,1], Joanna Kia Min Tan[b,c,1], Andrea L. Wong[a,d,e], Marie-Veronique Clement[f,g], Li Ren Kong[a], Naoto Ohi[h], Takeshi Tsunoda[i], Jianhua Qu[c], Boon Cher Goh[a,d,e,j,k,*], Shazib Pervaiz[c,g,j,l,*]

[a] Cancer Science Institute, National University of Singapore, Singapore 117599, Singapore
[b] Genome Institute of Singapore, Singapore 138672, Singapore
[c] Department of Physiology and Medical Science Cluster Cancer ProgramYong Loo Lin School of Medicine, National University of Singapore, Singapore 119753, Singapore
[d] Department of Hematology-Oncology, National University Health System, Singapore 119228, Singapore
[e] Department of Medicine, Yong Loo Lin School of Medicine, National University of Singapore, Singapore 119228, Singapore
[f] Department of Biochemistry, Yong Loo Lin School of Medicine, National University of Singapore, Singapore 117596, Singapore
[g] NUS Graduate School for Integrative Sciences and Engineering, Singapore 117456, Singapore
[h] Fujii Memorial Research Institute, Otsuka Pharmaceutical Co. Ltd., Shiga 520-0106, Japan
[i] Otsuka Pharmaceutical Co. Ltd., Tokyo 101-8535, Japan
[j] National University Cancer Institute, National University Health System, Singapore 119074, Singapore
[k] Department of Pharmacology, Yong Loo Lin School of Medicine, National University of Singapore, Singapore 117600, Singapore
[l] Curtin Health Innovation Research Institute and School of Pharmacy and Biomedical Sciences, Curtin University, Perth 6102, Australia

ARTICLE INFO

Keywords:
Metabolic reprogramming
OXPHOS
Oncogene-addiction
STAT3

ABSTRACT

The ability to selectively eradicate oncogene-addicted tumors while reducing systemic toxicity has endeared targeted therapies as a treatment strategy. Nevertheless, development of acquired resistance limits the benefits and durability of such a regime. Here we report evidence of enhanced reliance on mitochondrial oxidative phosphorylation (OXPHOS) in oncogene-addicted cancers manifesting acquired resistance to targeted therapies. To that effect, we describe a novel OXPHOS targeting activity of the small molecule compound, OPB-51602 (OPB). Of note, *a priori* treatment with OPB restored sensitivity to targeted therapies. Furthermore, cancer cells exhibiting stemness markers also showed selective reliance on OXPHOS and enhanced sensitivity to OPB. Importantly, in a subset of patients who developed secondary resistance to EGFR tyrosine kinase inhibitor (TKI), OPB treatment resulted in decrease in metabolic activity and reduction in tumor size. Collectively, we show here a switch to mitochondrial OXPHOS as a key driver of targeted drug resistance in oncogene-addicted cancers. This metabolic vulnerability is exploited by a novel OXPHOS inhibitor, which also shows promise in the clinical setting.

1. Introduction

The process of carcinogenesis and its progression is a functional outcome of dysregulation of several critical regulatory networks/pathways that maintain tissue and organ homeostasis. Thanks to the tremendous strides in the development of novel technologies and platforms, there has been an enormous advancement in our understanding of the processes involved in the various stages of cellular transformation, in particular, the tight balance between proteins products of genes that promote carcinogenesis and those that serve to suppress neoplastic transformation [1]. Notably, recent observations provide support to the hypothesis that a transformed cell might call on different sources of energy to keep up with the high anabolic needs from the point of initiation to expansion and progression of carcinogenesis [2–4]. In this regard, the preferred reliance on glucose as the essential source of carbon in cancer cells formed the basis for the Warburg effect. The relative increase in the shuttling of glucose-derived pyruvate to lactate during this switch is a function of induced expression of lactate dehydrogenase (LDH) even in the presence of oxygen and/or increased expression of pyruvate kinase M2 isoform (PK-M2)

* Corresponding authors at: National University Cancer Institute, National University Health System, Singapore 119074, Singapore.
E-mail addresses: boon_cher_goh@nuhs.edu.sg (B.C. Goh), Shazib_Pervaiz@nuhs.edu.sg (S. Pervaiz).
[1] Equal contribution.

https://doi.org/10.1016/j.redox.2018.101076
Received 13 November 2018; Received in revised form 30 November 2018; Accepted 11 December 2018

[5], which is not the only transcriptional target of hypoxia inducible factor-1α (Hif-1α) [5,6]. While the Warburg effect is a well-established phenomenon associated with the process of carcinogenesis, there is also evidence linking the activation of oncogenes, such as *Ras* and *Myc*, to an increase in mitochondrial OXPHOS [3]. Furthermore, there is also experimental evidence that mitochondrial metabolism is not entirely shut down but might exhibit significantly low to even appreciably high activity in cancer cells. This data suggests the possibility that different cell states during the process of carcinogenesis utilize disparate fuel sources to keep up with the increased metabolic demands. The latter is corroborated by a recent study by Yu et al., which postulates the existence of a "hybrid state", in which both metabolic modes coexist [7].

As a matter of fact, metabolic adaptions [8] have been reported to play a role in not only conferring resistance to targeted therapies in oncogene-addicted cancer cells, but also in the refractory behavior of cancer stem cells (CSCs). It is tempting to hypothesize that the activation of surrogate/compensatory survival networks, such as STAT3 [9], MET [10,11], and PI3K/Akt [12], as a mechanism of resistance to targeted therapies in oncogene-addicted cancer cells could be associated with metabolic reprogramming to a predominantly OXPHOS-driven milieu. Indeed, using several models of oncogene-addicted cancers with acquired resistance to oncogene-targeted therapy, such as TKI, we present evidence indicating reprogramming to a predominantly OXPHOS-dependent metabolism. Of note, in a search to identify small molecules with selectivity towards OXPHOS-driven cancers, we unravel a novel biological activity of a small molecule compound, OPB (Otsuka Pharmaceuticals) [13,14]. Oncogene-addicted cancers with acquired resistance to targeted therapy exhibit enhanced sensitivity to OPB via mechanisms that involve inhibition of mitochondrial oxygen consumption and complex I activity. More importantly, the clinical validation of the anti-tumor activity strongly suggests a novel therapeutic strategy for refractory cancers. Taken together, this data demonstrates that oncogene-addicted cancers reprogram their metabolism to predominantly OXPHOS-driven and highlight the tremendous therapeutic potential of exploiting this acquired vulnerability.

2. Results

2.1. Oncogene-addicted cancer cells with acquired resistance to targeted therapy exhibit elevated aerobic mitochondrial respiration

We first established cell line models of acquired resistance to targeted therapies, to identify common resistance mechanisms. HCC827 is an EGFR-mutant NSCLC cell line that is sensitive to the EGFR small molecule inhibitor, gefitinib, while A375 is a BRAF-mutant melanoma cell line that is sensitive to the BRAF small molecule inhibitor, vemurafenib. The respective cell lines were cultured with increasing concentrations of gefitinib or vemurafenib to obtain the gefitinib-resistant HCC827 cells (HCC827-GR) and the vemurafenib-resistant A375 cells (A375-VR) (Supp. Fig. 1A). NSCLC cell line H1975 has a T790M EGFR mutation, thus conferring inherent resistance to EGFR inhibitors. Given that up-regulated STAT3 signaling was reported as a compensatory resistance mechanism to targeted therapies [9], we explored this phenomenon in our model cell lines. Indeed, HCC827-GR and A375-VR cell lines displayed increased STAT3 phosphorylation at Tyrosine 705 (p-Tyr705) but not at serine 727 (p-S727) (Supp. Fig. 1B) and elevated levels of interleukin-6 [IL-6] (Supp. Fig. 1C). Notably, the therapy-resistant cell lines, HCC827-GR and A375-VR, elicited significant amplification in mitochondrial oxygen consumption [OCR] (Fig. 1A) compared to their parental counterparts, which is indicative of increased mitochondrial OXPHOS activity. To further corroborate the link between therapy resistance in oncogene-addicted cells and increased mitochondrial OXPHOS, we expanded our investigations to three other model systems, i.e., crizotinib-resistant H2228 cells (H2228-CR), T315I mutant BaF3 cells (BaF3T315I) and MDA-MB-231 triple negative breast cancer (TNBC) cells. Interestingly, increased basal OCR was consistently observed in H2228-CR and BaF3T315I cells (Fig. 1A) as well as in MDA-MB-231 cells (Supp. Fig. 1D), compared to their respective control cell lines. Furthermore, the switch to OXPHOS in the resistant cell lines could possibly be accounted for by the amplification in mitochondrial-DNA content [mtDNA] (Fig. 1B), increase in mitochondrial mass as evidenced by upregulation of PGC1α and TFAM expression (Fig. 1C) and appearance of complex I and II supercomplexes formation upon Blue-Native polyacrylamide gel electrophoresis (BN-PAGE) analyses of individual ETC (electron transport chain) complexes (Fig. 1D). Taken together, these data provide testimony that therapy-resistant oncogene-addicted cancers undergo reprogramming to an OXPHOS-driven metabolism.

2.2. Small molecule compound OPB is a novel OXPHOS inhibitor

Intrigued by the significant increases in STAT3 phosphorylation and mitochondrial OCR in oncogene-addicted therapy-resistant cancer cells, we set out to investigate if the increase in STAT3 phosphorylation associated with oncogene-addicted TKI resistance was also the effector mechanism triggering the metabolic switch to OXPHOS and more so if this cell state afforded enhanced sensitivity to pharmacological inhibitors of STAT3 and/or OXPHOS. To verify these possibilities we made use of two known pharmacological inhibitors of STAT3, Stattic [15] and OPB [14], and two OXPHOS inhibitors, elesclomol [16] and metformin [17]. Elesclomol was also identified in a high throughput screen comprising of Selleckchem® compound libraries (anti-cancer and epigenetics compound library) to selectively target HCC827-GR and A375-VR cells (Supp. Fig. 1E, Fig. 1E). Notably, OPB elicited much stronger inhibitory effects on mitochondrial respiration (Fig. 1F) and cell survival (Fig. 1G) in HCC827 and HCC827-GR cells than the other three compounds. In particular, the inhibitory effect of OPB on mitochondrial respiration was even superior to the commonly used mitochondrial complex I inhibitor, metformin (Fig. 1F). This is in agreement with a recent finding highlighting OPB induced mitochondrial dysfunction; however, the underlying mechanism described in that report implicated the SH2 domain of STAT3 [14]. To gain further insight into the OXPHOS inhibitory activity of OPB and its relationship to STAT3 signaling, we first confirmed using KINOMEscan™ scanMAX that OPB did not elicit significant off-target effects on a wide range of upstream kinases (Supp. Fig. 1F). Furthermore, similar to the results shown with HCC827-GR, OPB elicited significantly better survival inhibitory activity against A375-VR cells and BaF3T315I cells compared to the respective parental cell lines (Fig. 1H) as well as H1975 cells at relatively low (nanomolar) IC_{50} concentrations (Supp. Fig. 1G). The efficacy of OPB (in nanomolar range) was also validated in non-oncogene-addicted nasopharyngeal carcinoma cell lines HK-1 and C666-1 (Supp. Fig. 1H). This correlated with an inhibition of STAT3 phosphorylation at Y705 site (p-Tyr705) and IL-6 levels following OPB treatment (Supp. Fig. 1I) as well as inhibition of dimerization of STAT3 (Supp. Fig. 1J), which was previously reported as the mechanism of action of OPB. However, it is important to note that knockdown of *STAT3* failed to rescue cells from the growth inhibitory and OCR suppressing effects of OPB (Supp. Fig. 2A-C), thus corroborating the STAT3-independent mechanism of OXPHOS inhibition. Also, similar to the oncogene-addicted cell lines, *STAT3* knockdown did not rescue HK-1 cells from the inhibitory effects of OPB (Supp. Fig. 2D). Finally, OPB elicited striking in vivo potency in prolonging survival and reducing tumor burden in murine xenograft models (Fig. 1I, Supp. Fig. 3). These data lend credence to the possibility that the metabolic switch to OXPHOS is not only an independent mechanism of acquired-resistance but may also represent a vulnerability that is efficiently targeted by the small molecule compound, OPB.

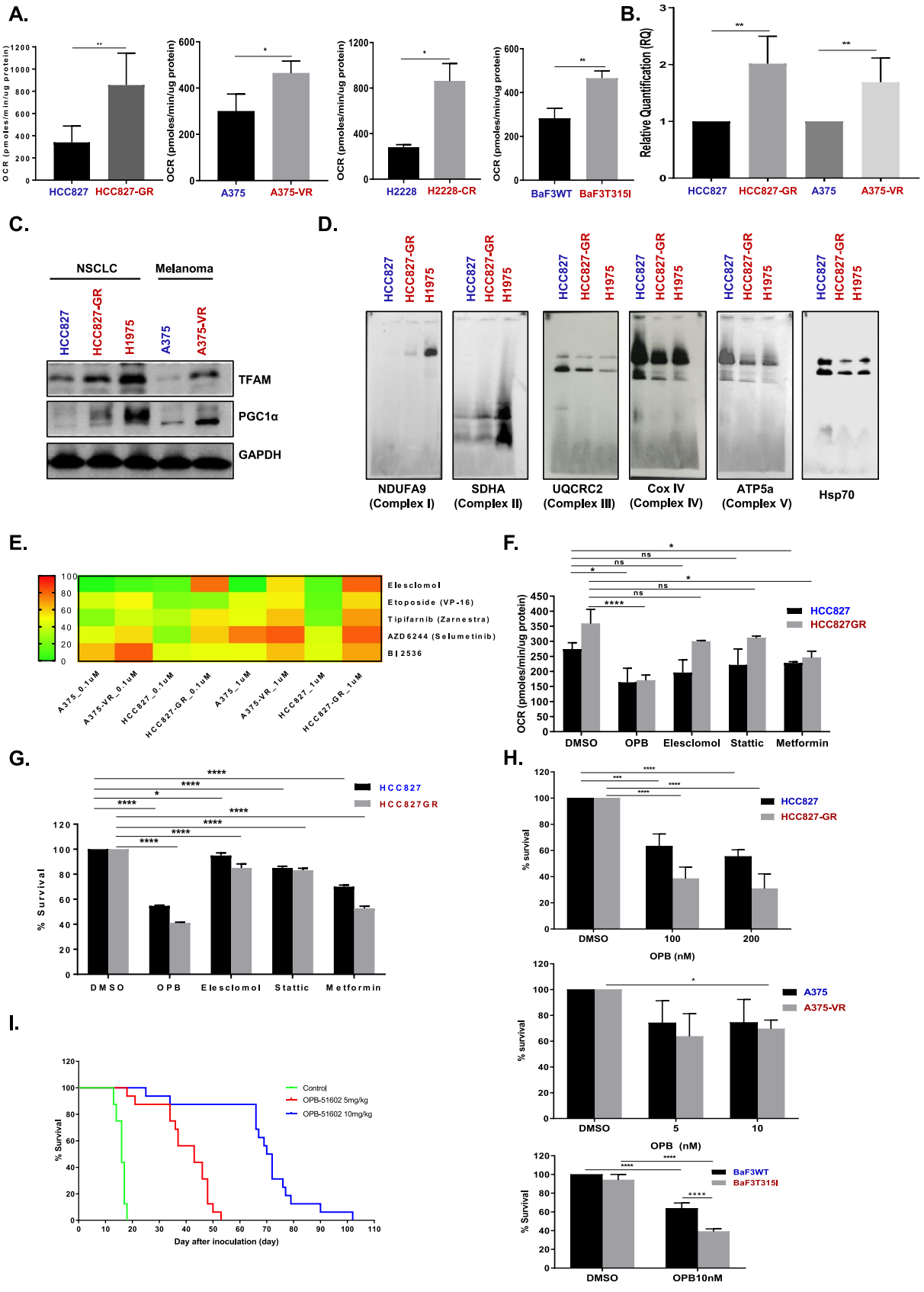

(caption on next page)

Fig. 1. ***Oncogene-addicted cancer cells with acquired resistance to targeted therapy exhibit elevated aerobic mitochondrial respiration and small molecule OPB inhibits OXPHOS***. (A) Basal OCR was measured using Seahorse Analyzer XF^{e}24 in HCC827, HCC827-GR, A375, A375-VR, H2228, H2228-CR, BaF3WT and BaF3T315I cells. (B) Mitochondrial DNA copy number was measured using qPCR and represented in terms of relative quantification (RQ) with HCC827 and A375 as control. (C) Basal TFAM and PGC1α expression levels were measured as an indication of mitochondrial biogenesis via western blot in HCC827, HCC827-GR, H1975, A375 and A375-VR cells with GAPDH used as a loading control. (D) Mitochondrial supercomplexes was checked via BN-PAGE using individual complex antibodies and HSP70 was used as a loading control. (E) Selleckchem Anti-cancer compound library (414 compounds, #L3000) and Epigenetic library (151 modulators, #L1900) were used for highthroughput chemical screening and cell viability were assayed using Celltiter-Glo luminescent. (F) HCC827, HCC827GR cells were exposed to 1 mM Metformin, 1 μM Elesclomol, 10 μM Stattic and 100 nM OPB for 4hrs before measuring OCR using Seahorse Analyzer XF^{e}24. (G) Cell viability was measured using crystal violet cell viability assay after 48 h exposure to 1 mM Metformin, 1 μM Elesclomol, 10 μM Stattic and 100 nM OPB in HCC827and HCC827-GR cells. (H) Cell viability was measured using crystal violet cell viability assay after 48 h of OPB treatment on HCC827, HCC827-GR, A375, A375-VR, BaF3WT and BaFT315I cells. (I) 5×10^6 U-937 cells/body inoculated in tumor-bearing mice and allocated to 3 groups of 16 each based on body weight on the day of the inoculation. OPB was orally administered once daily from the day after group allocation until death occurred. Figure shows the survival curve in each group calculated by the Kaplan-Meier method. Statistical differences were determined by log-rank test using the Bonferroni correction (by two independent tests) for multiple comparisons. P values in A, B, F, G and H were calculated by paired Student's t-test using GraphPad Prism. Therapy-resistant oncogene-addicted cell lines are shown in red font in this and subsequent figures.

2.3. Drug-resistant oncogene-addicted cells are metabolically reprogrammed to depend on OXPHOS for survival, representing a metabolic vulnerability to OXPHOS inhibition

Fluxes in OCR upon sequential addition of specific mitochondrial inhibitors and uncouplers are frequently used to indicate mitochondrial (dys)function [18]. Firstly, the effect of OPB on basal OCR was assessed. As shown in the earlier data, OPB treatment resulted in a significant drop in the basal OCR of the oncogene-addicted TKI-resistant cells (HCC827-GR, A375-VR and T315I, H396R and M315T mutation of Baf3) and their respective parental cells (Fig. 2A). Next, the maximum OCR upon dissipating the membrane potential with FCCP was assessed. Interestingly, OPB treatment also resulted in a significant decrease in maximum OCR (Fig. 2B), which was associated with a marked increase in Extracellular Acidification Rate (ECAR) in the various cell line models (Fig. 2C); increase in ECAR has been reported as a surrogate and suggestive indicator of mitochondrial respiration inhibition [19]. The latter was further corroborated by the significant increase in extracellular lactate levels in OPB-treated H1975 cells (Fig. 2D). Furthermore, the effect of OPB on OCR was also assessed in the presence of oligomycin (Oligo), FCCP, rotenone and antimycin A (Rot/AA), inhibitors of ETC complexes. Results indicate that exposure of H1975, HK-1 and C-666-1 cells for 1 h to OPB completely suppressed mitochondrial respiration with a reciprocal increase in ECAR (Fig. 2E-H). Lastly, as mitochondrial OXPHOS is dependent on the supply of oxygen for ATP generation, we evaluated the effect of hypoxia (4% O_2 as compared to 21% O_2) on OPB-induced inhibition of ATP production. Notably, while hypoxia was observed to reduce constitutive ATP levels, OPB-induced cessation of ATP generation/levels was abrogated under hypoxic states (Fig. 2I), thereby indicating the obligatory requirement of active OXPHOS machinery in the mitochondria targeting activity of OPB.

2.4. OPB mediates its effect on mitochondrial respiration through the specific inhibition of mitochondrial Complex I activity

So far, results provided evidence to link the anti-cancer activity of OPB to its inhibitory effect on mitochondrial OCR. Therefore, to further elucidate the exact mechanism involved in the specific targeting of oncogene-addicted cells that switch to OXPHOS for survival against drug-induced execution was assessed. To that end, analysis of the expression profile of OXPHOS-regulating genes showed a dose dependent downregulation of NDUFA9, NRF1, TFAM, PGC1α, and SOD2 in response to OPB (Fig. 3A). Coupled to that, analysis of mitochondrial ETC complexes by 2D SDS-PAGE following separation by BN-PAGE revealed a significant decrease in Complex I subunit, NDUFA9 (circled) as well as Complex II, IV and V (ATP Vα) (Fig. 3B). In addition, a significant increase in mitochondrial superoxide ($O_2^{\cdot-}$) was observed in cells following exposure to OPB (Supp. Fig. 4A), which further corroborates with the inhibitory effects of OPB on OXPHOS. Intrigued by these findings, we next set out to evaluate the effect of OPB on the activity of the five key complexes of the mitochondrial ETC. Using bovine heart mitochondria (BHM) as the standard for basal mitochondrial complex activity, the effect of increasing concentrations of OPB on each of the complexes was investigated. Notably, OPB exhibited inhibitory effect on complex I activity in BHM (Fig. 3C) as well as in H1975 cells (Fig. 3D), which was comparable to rotenone (Rot), a known complex I inhibitor. No significant effect was observed on the activities of the other four complexes (Supp. Fig. 4B), thereby indicating specific targeting of Complex I. The Complex I-specific effect of OPB was corroborated by the significant reduction in NAD^+/NADH ratio (Fig. 3E), a parameter commonly used as an indicator of Complex I activity (NADH dehydrogenase), as well as, by the signification reduction in the in-gel activity using BN-PAGE (Fig. 3F). The remarkable similarity between the effects of OPB and the bona fide complex I inhibitor, Rot, were also verified in the NPC cell line model. While OPB rapidly inhibited mitochondrial OCR, similarly as Rot, the further addition of Rot to OPB-treated cells displayed no further reduction in OCR (Fig. 3G). In addition, *a priori* treatment with OPB was sufficient to dose-dependently reduce basal OCR, with doses as low as 30 nM completely inhibiting mitochondrial OCR in the same NPC cells (Fig. 3H). These data provide sufficient evidence that the OCR regulatory activity of OPB is linked to its ability to strongly inhibit Complex I activity, which could in part be linked to the repression of the sub-unit, NDUFA9.

2.5. Cancer stem cells rely on OXPHOS for survival in drug-resistant oncogene-addicted cells and are sensitive to OPB inhibition

Stimulated by the novel OCR targeting activity of the small molecule compound OPB, we next set out to assess if the reported dependence of CSC on OXPHOS [20,21] could present as a vulnerability that might be exploited by specific OXPHOS inhibitors such as OPB. In this regard, we hypothesized that TKI-resistant OXPHOS-driven oncogene-addicted cells could have higher CSC populations. Indeed, results of microarray gene analyses confirmed CSC enrichment in the various models (HCC827, HCC827-GR, A375, A375-VR); heat map analysis revealed a significant increase in CSC-associated ALDH1 in the resistant cells (Fig. 4A). This observation was supported by higher level of ALDH1 in HCC827-GR and A375-VR, measured using CSC-specific markers (Supp. Fig. 5A, Fig. 4B). Notably, and in agreement with an earlier report [21], results showed that the CSC-enriched population ($ALDH1^+$ sorted cells from A375VR) exhibited significantly higher OCR compared to non-CSC population ($ALDH1^-$), and more importantly, OPB specifically and significantly inhibited OCR in the $ALDH1^+$ fraction (Figs. 4C and 4D). Along similar lines, $CD133^+$ CSC fractions isolated from A375-VR cells formed melanospheres (within seven days), which was significantly inhibited upon incubation with OPB (Fig. 4E).

In a separate set of experiments using MCF7 breast cancer cell line and the highly aggressive breast cancer cell line MDA-MB-231 cells as well as two malignant derivatives of the non-transformed MCF10A

breast cancer cells (MCF10A 1aBM and MCF10A 1hBM), we verified the association between stemness and OCR. Firstly, microarray analysis showed a significant increase in *CD44*$^{+}$*/CD24*$^{-}$*/EpCAM*$^{-}$ profile in MDA-MB231 cells compared to MCF7 (Fig. 4F). Secondly, both clones of MCF10A and MDA-MB-231 showed equal and significant sensitivity to OPB (Supp. Fig. 6). Notably, the CD44^{+}/CD24^{-}-sorted fraction within

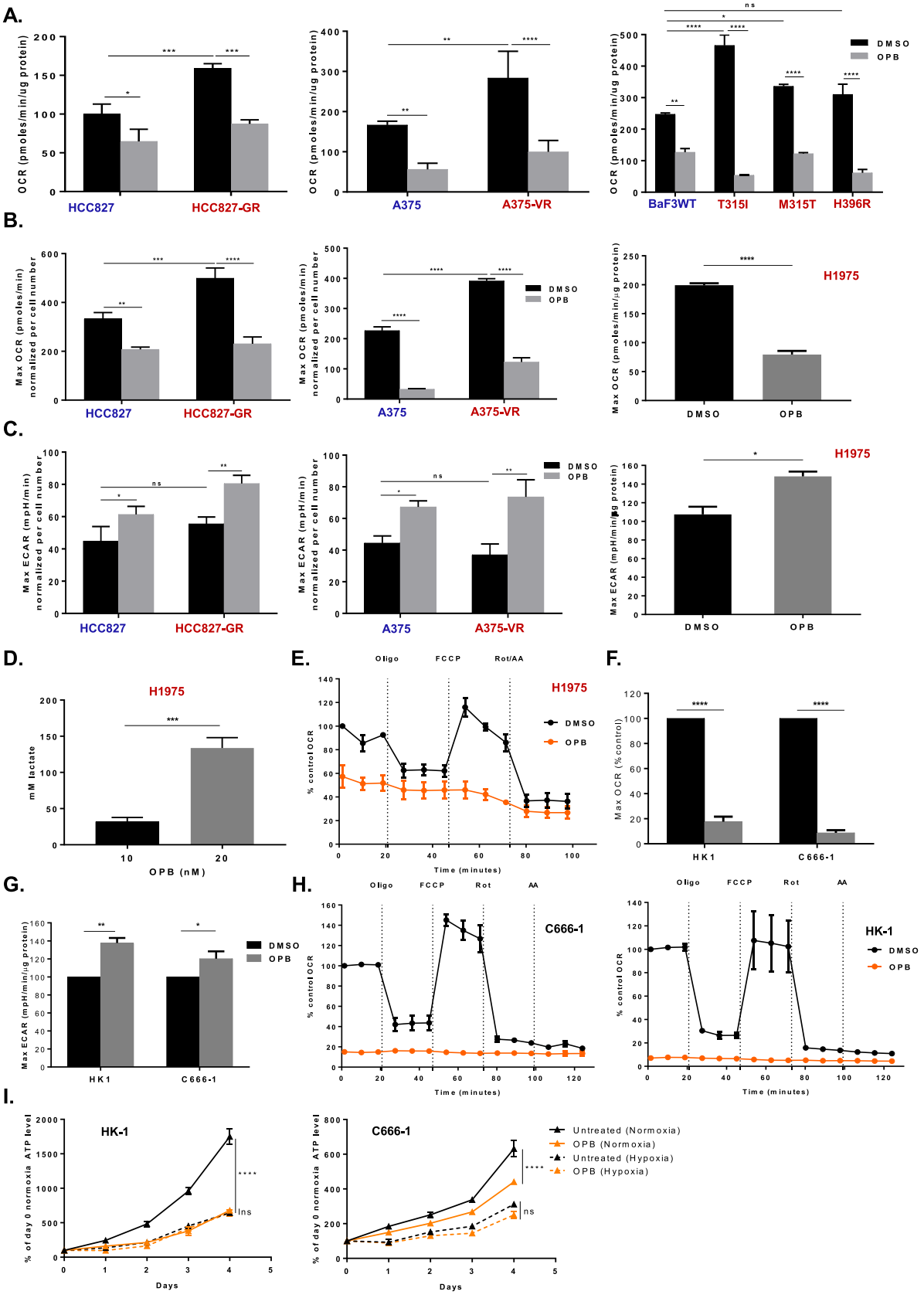

(caption on next page)

Fig. 2. ***OPB-51602 inhibits aerobic mitochondrial respiration and induces mitochondrial dysfunction.*** **(A)** HCC827, HCC827GR, A375, A375VR and BaF3 WT/T315I/M315T/H396R cells were exposed to 50 nM (HCC827/HCC827-GR), 20 nM (A375/A375-VR), and 10 nM (BaF3 cells) of OPB respectively for 1 h before measuring OCR using Seahorse Analyzer XF^{e}24. (N = 3) **(B)** Maximum OCR was measured using Seahorse Analyzer XF^{e}24 with FCCP in HCC827, HCC827GR, A375 and A375VR cells after exposing to 50 nM and 20 nM of OPB respectively for 1 h. (N = 3) **(C)** Maximum ECAR was measured using Seahorse Analyzer XF^{e}24 in HCC827, HCC827GR, A375, A375VR and H1975 cells after exposing to 50 nM (HCC827 and HCC827-GR) and 20 nM (A375, A375-VR and H1975) of OPB respectively for 1 h. (N = 3) **(D)** Lactate level was measured using lactate measurement kit in H1975 cells after exposing to different doses of OPB for 1 h. (N = 3) (E) OCR measurement was done on treated (20 nM OPB) and non-treated H1975 cells using Seahorse Analyzer XF^{e}24. Oligomycin (1 μM), FCCP (1 μM) and Rotenone/Antimycin A (Rot/AA) (1/0.5 μM) was used in injector to check different mitochondrial complexes **(F)** Maximum OCR was measured using Seahorse Analyzer XF^{e}24 with FCCP in HK-1 and C666-1 cells after exposing to 30 nM OPB for 1 h. (N = 3) **(G)** Maximum ECAR was measured using Seahorse Analyzer XF^{e}24 in HK-1 and C666-1 cells after exposing to 30 nM OPB for 1 h. (N = 3) **(H)** OCR measurement was done on treated (30 nM OPB) and non-treated HK-1 and C666-1 cells using Seahorse Analyzer XF^{e}24. Oligo (1 μM), FCCP (1 μM) and Rot/AA (1 μM/0.5μM) was used in injector to check different mitochondrial complexes **(I)** ATP level was detected in HK and C666-1 cells after exposing to 30 nM OPB in normoxic (21%O_2) and hypoxic (4%O_2) condition. Error bars shown as SD, *P* values in **A** were calculated by two ways ANOVA and **C-G** were calculated by paired Student's *t*-test.

the MDA-MB231 cells not only exhibited a significant increase in OCR but more importantly OPB virtually completely inhibited OCR in this fraction (Fig. 4G). In addition, a significant reduction in the $CD44^+$/$CD24^-$ fraction as well as inhibition of mammosphere formation were observed upon exposure to OPB (Fig. 4H-I), further corroborating the CSC targeting activity of the small molecule. Finally, the CD44/CD24 expression profiles (by flow cytometry) were obtained for the MCF10A1aBM and MCF10A1hBM cells before and after OPB treatment. Results show that exposure to OPB resulted in a significant left shift of the populations in MCF10A1aBM (21.04% vs 1.87%) and MCF10A1hBM (48.02% vs 0.59%), suggestive of specific targeting of CSC-like populations (Fig. 4J). Taken together, these data provide evidence for enrichment of CSC-like populations in oncogene-addicted drug-resistant cancers with a preference for OXPHOS-driven bioenergetics, and that this metabolic switch presents as a potential vulnerability exploited by the novel OXPHOS inhibitor, OPB.

2.6. OXPHOS inhibition re-sensitizes cancer cells with acquired resistance to the respective targeted therapies

Having demonstrated a specific OXPHOS inhibitory activity of OPB with potential therapeutic targeting of CSC-enriched, oncogene-addicted TKI-resistant cancers, we next set out to evaluate the efficacy of low dose OPB in combination regimens. This is imperative based on the observations and our current data (Fig. 2C and D) indicating that monotherapy with relatively high doses of OXPHOS inhibitors could have potential off target effects, in particular, increases in ECAR and lactic acidosis. Therefore, we made use of the glycolysis inhibitor, 2-Deoxy-D-glucose (2-DG), as a single agent and in combination with OPB. Our results show that, while treatment of cells with 2-DG alone did not have a significant effect, the presence of 2-DG significantly amplified the response of cells to OPB (Supp. Fig. S7), indicating a strong synergistic effect. Notably, 2-DG also resulted in significantly inhibiting the increased ECAR associated with OPB treatment. To further validate, the combination of low concentrations of OPB with gefitinib and vemurafenib were assessed, particularly against cell lines that were rendered resistant to the specific TKIs (H1975, HCC827-GR and A375-VR). Strikingly, while all cell lines retained their selective resistance to the specific TKI, *a priori* treatment for 1 h with doses of OPB as low as 5–50 nM was sufficient to re-sensitize resistant cells to their respective targeted-therapies, as assessed by tumor colony formation (Fig. 5A), spheroid formation (Fig. 5B), and cell survival (Fig. 5C).

2.7. OPB exerts potent anti-tumorigenic effects in vivo

Based on our findings and earlier reports, cancers with reprogrammed reliance on OXPHOS rather than glycolysis for energy needs will possess greater sensitivity to OXPHOS inhibitors. Therefore, as a clinical validation of the effectiveness of OXPHOS inhibition in oncogene pathway driven tumors, we evaluated an extension cohort of patients with EGFR mutation positive NSCLC in a phase I study, which we previously reported [13]. In this group of patients with secondary resistance to EGFR TKIs, OPB treatment resulted in significant tumor size reduction on compound tomography [CT] (Fig. 6A) as well as metabolic response on ^{18}F-Fluoro-deoxyglucose positron emission tomography [FDG-PET] (Fig. 6B). In addition, another patient with imatinib refractory *c-kit* mutation positive gastrointestinal stromal tumor had a FDG-PET response to an OXPHOS inhibitor (Fig. 6C). Finally, supporting the in vitro effect of OPB in NPC cells, we observed good metabolic responses in a 29-year-old female with heavily pre-treated platinum-resistant NPC whose baseline FDG-PET imaging demonstrated multiple highly FDG-avid metastatic sites. Imaging performed after 3 weeks of OPB therapy showed significant reduction in metastatic lesions (Fig. 6D). These data not only corroborate the in vitro findings but also provide a clinical proof of concept highlighting the potential of OXPHOS targeting strategies in therapy-resistant oncogene-addicted tumors.

3. Discussion

Cancers are now thought to be flexible with regards to acquiring fuel to drive growth and may shift from anaerobic respiration to oxidative phosphorylation in response to increased energy needs. Identification of this metabolic shift may provide a vulnerability that can be exploited with OXPHOS inhibitors. Our current data suggests that with the development of resistance to oncogenic pathway inhibition in oncogene-dependent cancers, OXPHOS is upregulated to drive cellular bioenergetics, and this can be therapeutically addressed by an OXPHOS inhibitor. This finding may not be isolated to molecular pathway specific tumors; in certain cancers, like EBV-driven NPC, OXPHOS may represent a viable target for drug development. Supported by the promising metabolic responses in several patients with relevant clinical contexts in the clinical trials, inhibition of OXPHOS and metabolites [22] may indeed be a promising new direction for therapeutic drug development for drug-resistant cancers.

Previously, investigators have shown that in oncogene-addicted cancers, feedback upregulation of STAT3 activation via the IL-6/JAK and FGF/PI3K pathways represents a generalizable mechanism for resistance to molecular pathway specific inhibition that could be exploited therapeutically [9]. Further work by Genini *et al.* showed that OPB binds to the SH2 domain of STAT3 with high affinity, leading to a mitochondrial STAT3-drug interaction, which mediates mitochondrial dysfunction through accumulation of proteotoxic aggregates that ultimately leads to cell death [14]. Our work provides evidence for a novel OXPHOS inhibitory activity of OPB, independent of STAT3, in drug-resistant oncogene-addicted cancer cells. Furthermore, exposure to hypoxic conditions completely abolished the growth inhibitory effect of OPB, indicating that active OXPHOS machinery is crucial for drug-sensitivity. Hence, we postulate that the mechanism-of-action of OPB may be context-dependent and demonstrate here that direct mitochondrial complex I inhibition is the key target in cell lines which rely on OXPHOS for survival.

To explain the enhanced sensitivity to OXPHOS inhibition, we

identified enrichment in the CSC gene expression signatures in drug-resistant cells compared to their parental sensitive cells. This is concordant with the known metabolic switch to OXPHOS to provide augmented energy needs in CSC during cell expansion. These CSC populations were functionally reliant on OXPHOS for survival and hence susceptible to eradication by OPB. These findings are particularly

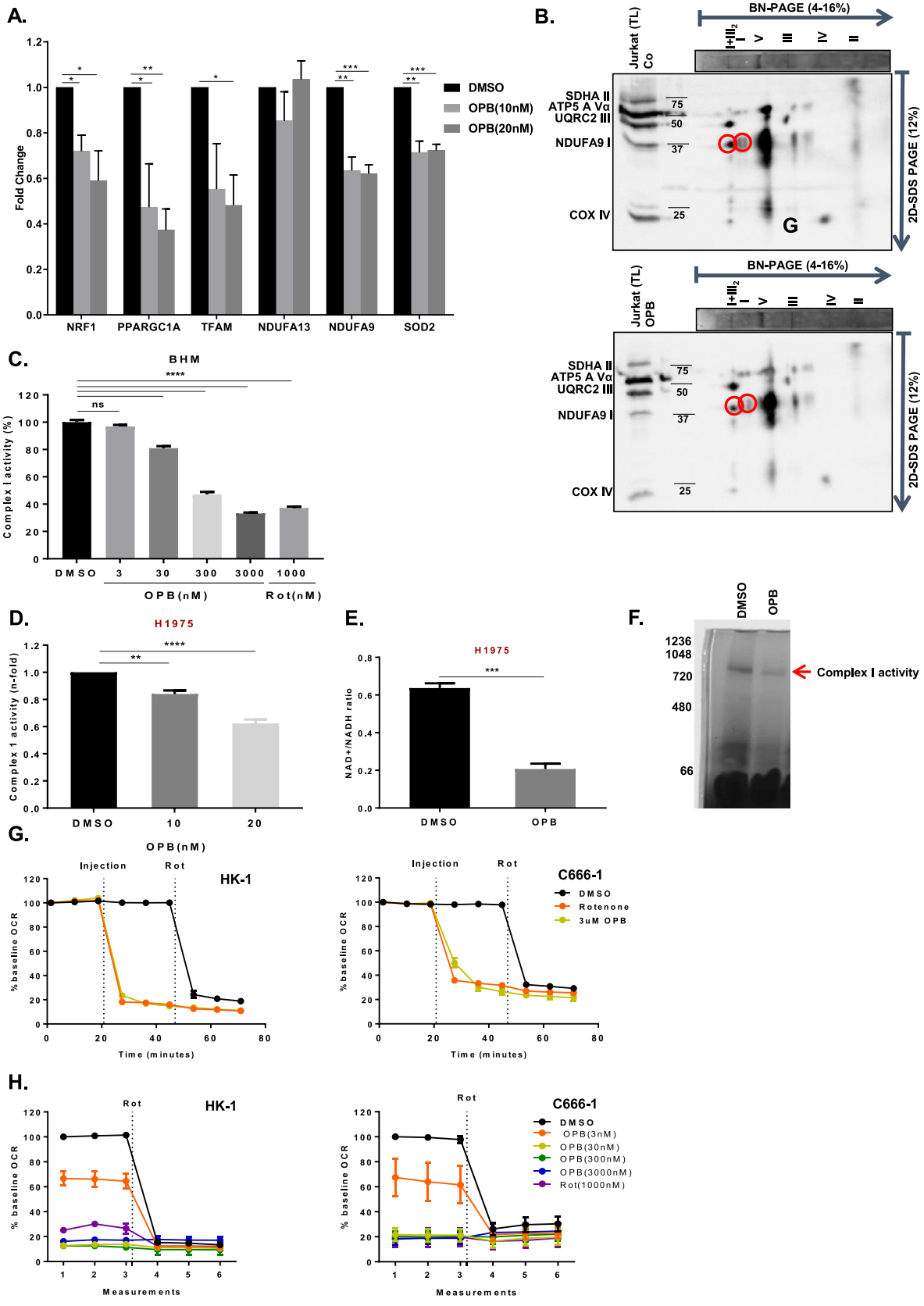

(caption on next page)

Fig. 3. ***OPB-51602 specifically inhibits mitochondrial complex I activity.*** **(A)** OXPHOS regulated genes were analyzed using RT^2 PCR Profiler Array in H1975 cells after exposing the cells to 10 nM and 20 nM OPB for 48 h. (N = 3) **(B)** 2D gel electrophoresis was done after running BN-PAGE with mitochondrial lysates of untreated Jurkat cells and Jurkat cells treated with 20 nM OPB. Membranes were probed with mitochondrial complex cocktail antibody (Abcam) to detect different mitochondrial respiratory complexes. **(C)** Mitochondrial complex I activity was measured using Complex I activity assay kit on bovine heart mitochondria (BHM) after exposing mitochondria with different concentrations of OPB and rotenone was used as a positive control. (N = 3) **(D)** Mitochondrial complex I activity was measured in H1975 cells using complex I activity assay after treating the cells with 10 nM and 20 nM OPB for 1 h. (N = 3) **(E)** NAD^+/NADH ratio was measured using NAD^+/NADH kit in H1975 cells treated and non-treated for 1 h with 20 nM OPB. (N = 3) **(F)** In-gel complex I activity was measured using BN-PAGE after H1975 cells were exposed to 20 nM OPB. **(G)** Time kinetics OCR was measured in HK-1 and C666-1 cells with separate injection of rotenone and OPB. **(H)** Time kinetics OCR was measured in HK-1 and C666-1 cells with separate injection of rotenone and different concentrations of OPB. Time interval between 2 measurements in the Y axis is 9 min. Error bars shown as SD, *P* values in **A, D** and **F** were calculated by paired Student's *t*-test.

noteworthy because many tumors are thought to harbor CSCs, which are notoriously resistant to standard anti-cancer therapies and are postulated to be critical drivers of cancer relapse and metastasis [23,24]. This phenomenon has recently been described in hematopoietic stem cells (HSCs), which largely remain quiescent in relatively hypoxic tumor microenvironments and heavily rely on anaerobic glycolysis. However, when HSCs undergo cellular differentiation, there is a rapid switch to an OXPHOS-upregulated state in order to meet the metabolic needs of the cell [25]. In BCR-ABL oncogene-driven chronic myeloid leukemia (CML), cells that were not eliminated by primary TKI therapy were enriched in CSC and susceptible to OXPHOS inhibition [20]. In this regard, reprogramming to OXPHOS dependence occurs as a generalizable survival mechanism regardless of the resistance mutation acquired in different cellular contexts, giving credence to OXPHOS as a target of resistance cells. Given that initial response to targeted therapy for oncogenic pathway driven malignancies is almost always temporary and acquired resistance inevitably develops, this finding of OXPHOS dependence is an exciting novel therapeutic strategy. Notably, recently, evidence is emerging on the importance of OXPHOS in mediating resistance to chemotherapy (docetaxel, etc) [26].

Despite prior efforts to develop OXPHOS inhibitors, there have been challenges posed by unfavorable clinical pharmacology, lack of biological activity and predictive biomarkers, and difficulty in achieving tumor-selective cytotoxicity. One of the main obstacles is in the identification of highly-specific enzymatic inhibitors of bioenergetics pathways [27]. There are presently very few OXPHOS inhibitors with specific anti-cancer indications in clinical use or in the developmental pipeline for tumors. Metformin possesses mitochondrial complex I inhibitory effects, which has led to significant efforts in repurposing it as an anti-neoplastic agent [28,29]. However, it has yet to be determined if the administration of metformin at clinically tolerable doses will achieve sufficient drug levels in neoplastic tissue [30,31]. In this context, our observations of clinical and imaging responses to OPB in the appropriate malignancies that have developed resistance to specific molecular targeted TKI treatment are highly encouraging. In theory, OXPHOS inhibitors should drive cellular metabolism towards glycolysis, which is expected to increase lesional FDG avidity on PET imaging. Hence, we concluded that the FDG-PET responses observed in our patients after several weeks of treatment are representative of genuine anti-tumor activity of the compound, rather than a mere pharmacodynamics effect. However, we have observed that lactic acidosis, an on-target effect on OXPHOS, is a potentially dose-limiting adverse event, but our further preclinical work that demonstrates synergistic effect of OPB with the glycolytic inhibitor and relevant oncogenic pathway inhibitor potentially allows clinically tolerable doses to be evaluated in combination therapy in future clinical trials.

In summary, we have characterized metabolic reprogramming as a mechanism of acquired resistance to targeted therapies and cancer stem cell survival, highlighting its potential as an Achilles heel in cancer medicine. This metabolic vulnerability was successfully targeted with a novel mitochondrial complex I inhibitor, paving the way for the clinical development of OXPHOS inhibitors (Fig. 6E).

4. Materials and methods

4.1. Cell culture and transfection

H1975, HCC827-WT and HCC827-GR, HK1, C666-1, BaF3, H2228-WT, H2228-CR and Jurkat cells were cultured in RPMI-1640 media (Hyclone), while A375, A375-VR and MDA-MB-231 were cultured in DMEM high glucose media (Hyclone); all the media were supplemented with 10% fetal bovine serum (FBS), 1% penicillin-streptomycin and 1% L-glutamine. Dr. Brian Druker (Oregon Health & Science University, USA) has generously provided BaF3 mutant P210 WT, P210 T315I, P210 M351T, P210 H396R cells. To maintain resistance to their respective drugs, cells were continuously cultured with 2 μM gefitinib (HCC827-GR), 2 μM vemurafenib (A375-VR) and 5 μM crizotinib (H2228-CR). All cells were kept at 37 °C with 5% CO_2. For assays under hypoxia, HK1 and C666-1 cells were subjected to 4% O_2 and processed swiftly following removal from hypoxia incubator. Transfection of HCC827, H1975 and HK-1 was performed using Dharmafect transfection reagent (Dharmacon, USA). 24 h after transfection, cells were washed and lysed using 1X cell lysis buffer (Cell Signaling, USA) supplemented with Protease and phosphatase inhibitor cocktail (Calbiochem, USA). The cells were lysed and cell lysates were stored at −80 °C before analyses by western blot.

4.2. Generation of TKI-resistant Cell Lines

HCC827 cells were treated with increasing doses of gefitinib (from 1 μM to 10 μM) for 48 h to obtain the IC_{50} of gefitinib in the cell line. Subsequently, the cells were cultured in T75 flasks with a starting dose of 0.5 μM gefitinib and maintained at 2 μM gefitinib in the culture once the cells (HCC827-GR) had developed resistance to the TKI. A375 cells were treated with increasing doses of vemurafenib (from 0.1 μM to 2 μM) for 48 h to obtain the IC_{50} of vemurafenib in the cell line. Subsequently, the cells were cultured in T75 flasks with a starting dose of 0.1 μM vemurafenib and maintained at 2 μM vemurafenib once the cells (A375-VR) had developed resistance to the TKI. H2228 cells were treated with increasing doses of crizotinib (from 0.5 μM to 20 μM) for 48 h to obtain the IC_{50} of crizotinib in the cell line. Subsequently, the cells were cultured in T75 flasks with a starting dose of 1 μM crizotinib and maintained at 5 μM crizotinib in the culture once the cells (H2228-CR) had developed resistance to the TKI.

4.3. Blue native and 2D gel electrophoresis

Mitochondrial fractions were dissolved using buffer A (200 mM Mannitol, 68 mM Sucrose, 50 mM Pipes-KOH pH 7.4, 50 mM KCL, 5 mM EGTA, 2 mM $Mgcl_2$ and 1 mM DTT) and loaded onto precast 4–16% Blue native gel (Bio-Rad), which were incubated with NADH for 1 h on an orbital shaker in the presence of Nitrotetrazolium blue (NTB) (Sigma-Aldrich, USA). Images were taken using Chemidoc software and equipment (Bio-Rad, USA). A second gel strip was cut and loaded onto a 12% SDS-polyacrylamide gel for separation and membrane transfer as detailed under immunoblotting.

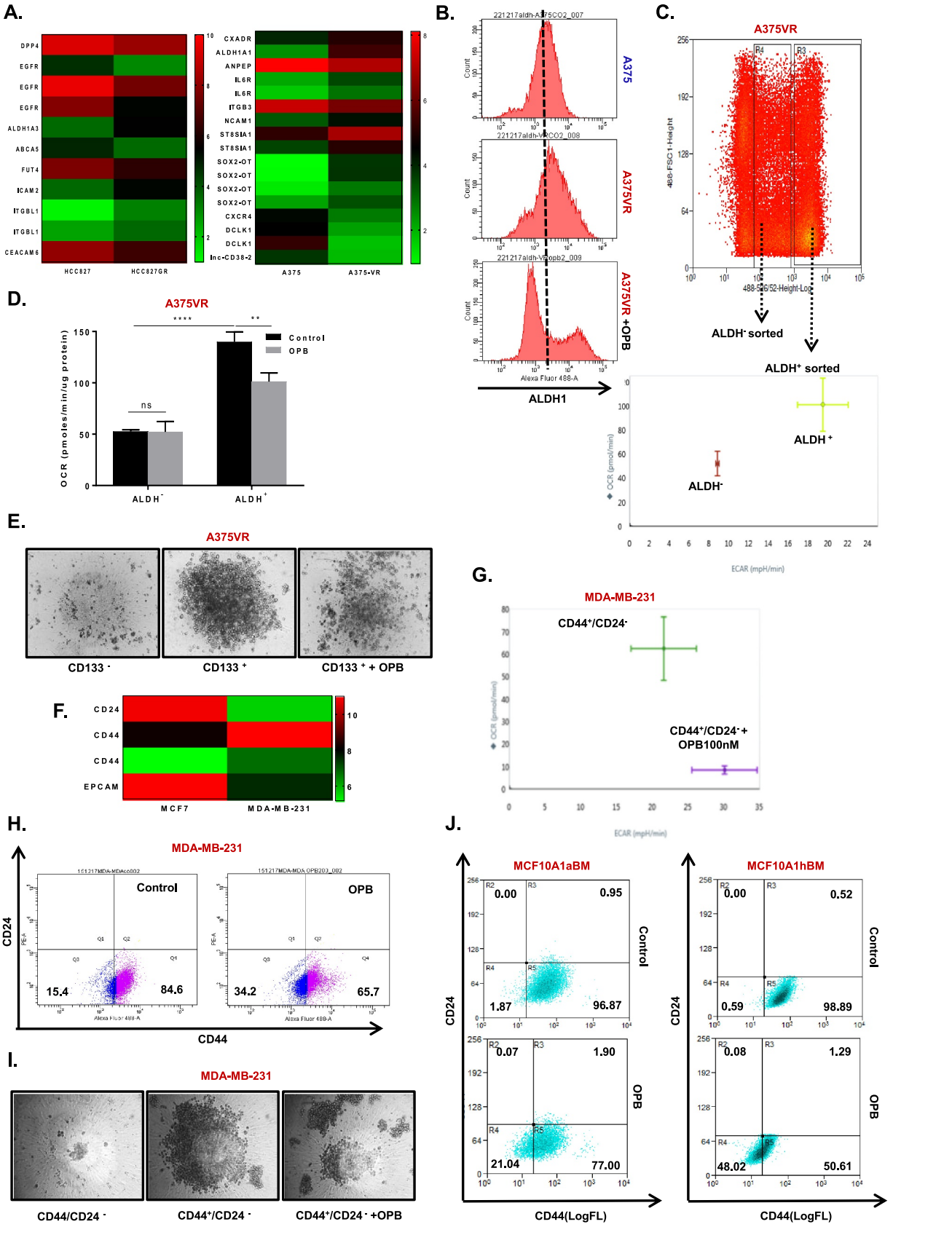

(caption on next page)

Fig. 4. ***OPB inhibits cancer stemness in increased CSC population in therapy-resistant oncogene-addicted cells.*** **(A)** Microarray analysis was done in HCC827, HCC827-GR, A375 and A375-VR cells using Agilent platform. **(B)** ALDH level was detected using flow cytometry in A375 basal level and in A375-VR after exposing to 20 nM OPB for 48hrs. **(C) & (D)** $ALDH^+$ and $ALDH^-$ populations were sorted in A375VR cells using FACS and the sorted cells were plated and OCR was measured in both populations after exposing the cells to 20 nM OPB for 1 h. (N = 3) **(E)** 2000 sorted cells of $ALDH^+$ and $ALDH^-$ population of A375VR were plated for spheroid formation, untreated and treated spheroids with 20 nM OPB for 7 days; Spheroids were imaged using ZEISS microscope. **(F)** Microarray analysis was done in MCF-7 and MDA-MB-231 cells using Agilent platform. **(G)** $CD44^+/CD24^-$ cells were sorted using flow cytometry, sorted cells were plated and OCR was measured in $CD44^+/CD24^-$ after exposing with 100 nM OPB. **(H)** CD44 and CD24 levels were measured by flow cytometry in MDA-MB-231 cells after cells were exposed to 200 nM of OPB for 48hrs. **(I)** 2000 sorted cells of $CD44^+/CD24^-$ +ve and $CD44^+/CD24^-$ -ve population of MDA-MB-231 were plated for spheroid formation, spheroids were treated 100 nM OPB for 7days and imaged using ZEISS microscope. **(J)** CD44 and CD24 level was measured by flow cytometry in MCF10A cells after cells were exposed to 100 nM OPB for 48hrs. Error bars shown as SD, *P* values in **D** were calculated by paired Student's *t*-test.

4.4. OCR and ECAR measurements

Cells were plated at respective optimal densities in Seahorse XF 24-well plates one or two days prior to the measurement. These were subjected to the stated conditions, and incubated in Seahorse XF Assay Media at 37 °C for 1 h without CO_2 just before running the assay. Final drug concentration was stated in Figures wheres substrate concentrations were 1uM for Oligo and FCCP, 1uM/0.5uM for Rot/AA and 5mM for succinate. All the reagents for OCR and ECAR were purchased from Seahorse Bioscience. OCR and ECAR measurements were obtained using the Seahorse XF^e24 Analyzer, and normalized to protein concentration (μg/μL).

4.5. CSC population

HCC827/HCC827GR and A375/A375VR cells were stained with ALDH using ALDHFLUOR kit (StemCell Technologies, Canada) according to manufacturer's instruction. MDA-MB-231 and MCF10A1aBM cells were stained with CD44 and CD24 for 30 mi. in wash buffer (0.5% BSA, 2 mM EDTA in phenol free medium) at 4°C and then analyzed in FACScalibur flow cytometer (BD LSR Fortessa). CD133, ALDH, CD44 stained cells were sorted after staining using Backman Coluter Moflow Astrios.

4.6. Human IL-6 Enzyme-linked Immunosorbent Assay (ELISA)

Cell culture media of target cells were collected into microcentrifuge tubes and spun down at 1500 rpm for 10 min at 4 °C to remove any cellular debris. The resulting supernatant was transferred to a new tube and subjected to manufacturer's instructions of the Human IL-6 ELISA Kit (Thermo Fisher Scientific, USA).

4.7. MtDNA quantification via qRT-PCR

Cells were collected and rinsed with PBS (1 ×) before lysing with total nucleic acid lysis buffer. 1 vol of phenol (Sigma-Aldrich, USA) was added and mixed gently on GyroMixer for 15 min at room temperature, prior to centrifugation at 14,000RPM for 5 min. After centrifugation, the aqueous top layer was transferred to a fresh eppendorf tube and 1 vol of chloroform: isoamyl alcohol 24:1 was added to the tube. The tubes are mixed gently for 15 min at room temperature, prior to centrifugation at 14,000RPM for 5 min. After centrifugation, the aqueous top layer was transferred to a fresh eppendorf tube and 0.2 vol of 5 M NaCl and 0.7 vol of isopropanol were added to the tubes and incubated on ice for 10 min until DNA pellet was visible. The tubes were centrifuges at 14,000RPM at 4 °C for 5 min, the supernatant was removed and DNA pellet was air dried. The DNA pellet was resuspended in 10 mM Hepes-NaOH buffer (pH 7.2) and DNA concentration was measured using Nanodrop 2000 (Thermo Fisher Scientific, USA). qPCR was performed using SYBR™ Select Master Mix from Thermo Scientific according to the manufacturer's instructions. Relative quantification (RQ) was calculated from Comparative ΔΔCT method. HPRT was used as internal normalization control.

4.8. Co-immunoprecipitation and immunoblotting

Following 4 h of 20 nM OPB treatment, H1975 cells were lysed in IP buffer (150 mM Nacl, 50 mM Tris-HCL pH 7.4) supplemented with 50 μM digitonin. Protein estimation was done using Coomasie Plus (Bradford) Protein Assay (Thermo Fisher Scientific, USA). 1 mg of protein was used to pull down GRIM19 and NDUFA9 after preclearing using Agarose A beads. Interacting proteins were then detected by immunoblotting as described below. Lysates were denatured in loading buffer and resolved on 10% sodium dodecyl sulfate-polyacrylamide gel electrophoresis (SDS-PAGE) followed by transfer to PVDF membranes using wet transfer method. The membrane was blocked with 5% non-fat milk for an hour at room temperature on shaker before probing it with appropriate primary antibodies overnight at 4 °C. The membrane were washed thrice with TBS + 0.1% Tween 20 before probing with the isotype specific secondary IgG-HRP for an hour. After washing with TBS + 0.1% Tween 20 membranes were exposed to EZ-ECL substrate Western Blotting Kit (Pierce, Rockford, IL, USA) and signal were detected using iBright Chemidoc (Thermo Fisher Scientific, USA).

4.9. Reagents and antibodies

For STAT3 knockdown using siRNA, following targeting ON-TARGETplus set of 4 SiRNA sequences (Dharmacon, USA) were used: 1. GAGAUUGACCAGCAGUAUA, 2. CAACAUGUCAUUUGCUGAA, 3. CCA ACAACCCAAGAAUGU, 4. CAACAGAUUGCCUGCAUUG

The following primers were used to check mitochondrial DNA copy no: mtDNA, Forward primer: CCTCCTCCTAGCAGCAGC, Reverse primer: GGTTGTGGATGATGGACCCG; HPRT, Forward primer: CCTGG GGATTCCAAATACCT, Reverse primer: GGGCAGAAAAGGTCATCAAA.

The following antibodies were used for immunoblotting: S727STAT3, STAT3 (Cell signaling, USA), GAPDH, β-actin, and VDAC-1 (Santa-Cruz, Dallas, TX), Y705STAT3, OXPHOS cocktail antibody, mtTFA, PGC1α, NDUFA9, GRIM19 (Abcam, Cambridge, UK), CD44, CD24, CD133 (BD Bioscience), FLAG, HA (Sigma-Aldrich, USA)

4.10. Crystal violet viability assay, 2D colony formation, and tumor spheroids formation assay

Approximately 100,000 to 200,000 cells were seeded onto 12-wells plates. 24 h after plating, cells were pre-treated with OPB for one hour. Subsequently, gefitinib (on H1975, HCC827, HCC827-GR) or vemurafenib (on A375 and A375-VR) were added for total treatment duration of 48 h. The treated cells were collected via trypsinization and re-seeded at approximately 2000 cells/well in either 6-well plates (2D Colony Formation Assay) or Corning® Spheroids 96-Well Microplates (Tumor Spheroids Formation Assay). 2000 sorted $CD133^+$ and $CD44^+/CD24^-$ cells were plated per well for spheroid formation from A375VR and MDA-MB-231 cell line respectively. Spheroids and colonies formed after 6 and 14 days respectively were imaged using the ZEISS® Axio Vert. A1 Microscope.

4.11. High throughput screening

Selleckchem Anti-cancer compound Library (414 compounds, #L3000) and Selleckchem Epigenetic Library (151 modulators, #L1900) were used for high-throughput chemical screening. All compounds were dissolved in Dimethyl sulfoxide (DMSO, Sigma Aldrich, USA). Approximately 1500 cells were seeded per well into a 384-well plate 24 h prior to drug treatment. For high throughput studies, cultures

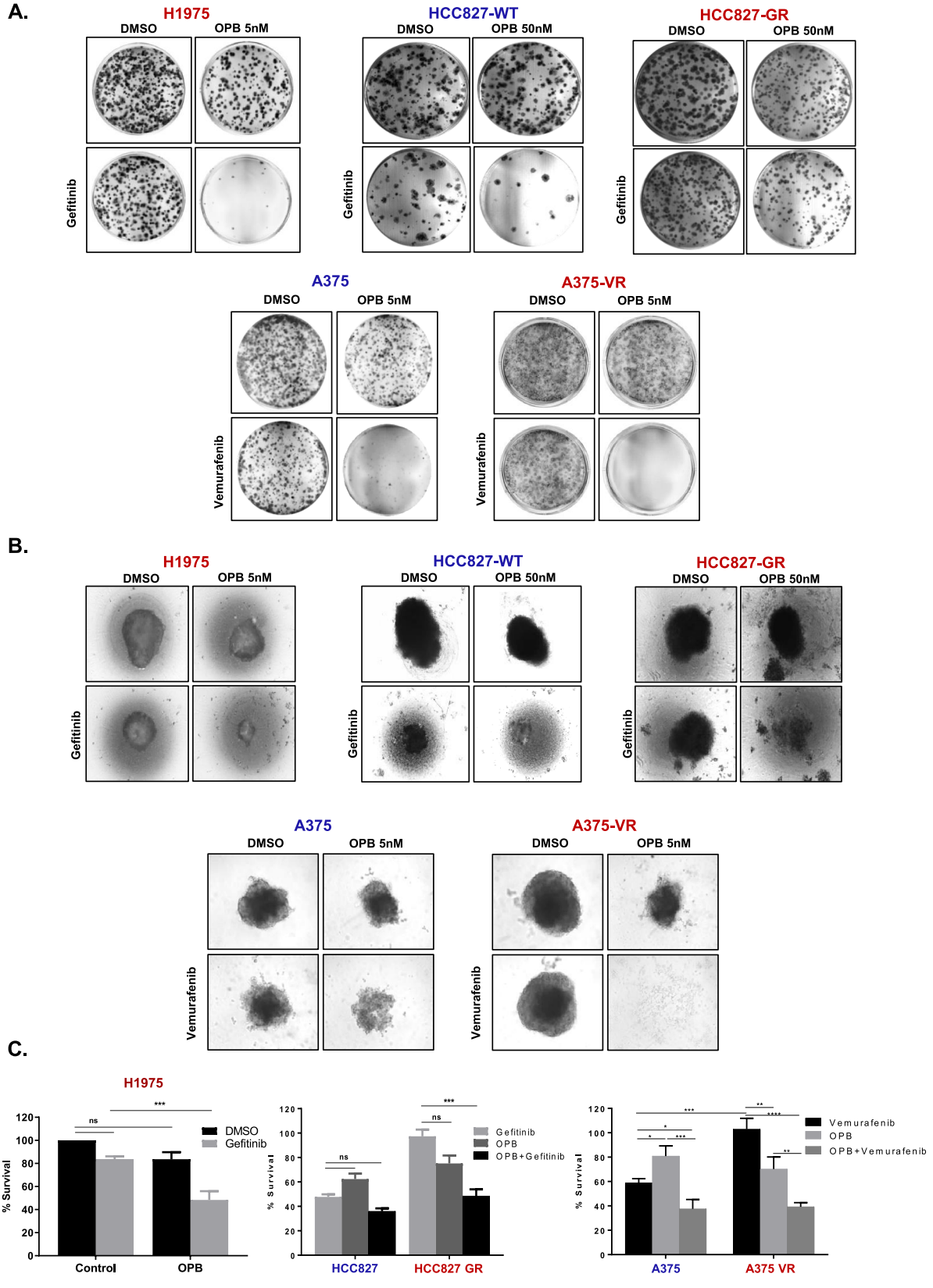

(caption on next page)

Fig. 5. ***Greater OPB sensitivity in oncogene-addicted cancer cells can be exploited for resensitization to targeted therapies*** **(A)** 2000 cells were plated in 6-wells plate for long term colony formation assay after H1975, HCC827, HCC827-GR, A375 and A375-VR cells were exposed to different concentrations of OPB for 1 h followed by 5 μM gefitinib (H1975), 0.5 μM gefitinib (HCC827 and HCC827-GR) and 0.4 μM vemurafinib (A375 and A375-VR) respectively for a total of 48hrs. Colonies were stained with crystal violet after 10 days of plating. **(B)** 2000 cells were plated in 96-wells Corning® spheroids plates after H1975, HCC827, HCC827-GR, A375 and A375-VR cells were exposed to different concentrations of OPB for 1 h followed by 5 μM gefitinib (H1975), 0.5 μM gefitinib (HCC827 and HCC827-GR) and 0.4 μM vemurafinib (A375 and A375-VR) respectively for a total of 48hrs. Spheroids were imaged using ZEISS microscope. **(C)** Cell viability was determined using MTT cell viability assay in H1975, HCC827, HCC827-GR, A375 and A375-VR cells after exposing to OPB for 1 h followed by 5 μM gefitinib (H1975), 0.5 μM gefitinib (HCC827 and HCC827-GR) and 0.4 μM vemurafinib (A375 and A375-VR) respectively for a total of 48hrs. (N = 3) Error bars shown as SD, *P* values in **C** were calculated by paired Student's *t*-test.

were dispensed (50 μL) into 384-well plates using a MultiFlo dispenser, while drugs were 100-fold diluted in DMSO and kept at 1% (v/v) across all drug concentrations and control. The viability of cells was assayed using CellTiter-Glo luminescent (Promega, USA) after 72 h of treatment. The luminescence signals were detected using TECAN Infinite M1000 pro multi-mode plate reader using an integration time of 250 ms.

4.12. Measurements of lactate concentrations, Complex I activity, and NAD +/NADH ratio

Lactate concentrations were obtained using the Lactate Assay Kit (Abcam, Cambridge, UK), following 20 nM OPB treatment in H1975 cells. H1975-specific Complex I activity was measured using the Complex I assay kit (Mitoscience, USA) following 1 h treatment of 10 and 20 nM OPB. Complex-specificity of OPB was tested on bovine heart mitochondria using a range of OPB concentrations on the MitoTox™ Complete OXPHOS Activity Assay Kit (Abcam, Cambridge, UK); a complex-specific inhibitor was included as a positive control. The NAD +/NADH ratio in H1975 was determined using the NAD+/NADH kit following 1 h of 20 nM OPB treatment.

4.13. Animal work methodology

Female C.B-17/Icr-scid/scid Jcl mice were subcutaneously inoculated with 5×10^6 HuH-7 and SW-620,10×10^6 SNU-1, 8×10^6 HuH-28, 5×10^6 MDA-MB-231 and Caki-1, 10×10^6 H1299, 50×10^6 kG-1, 30×10^6 BALL-1, and 1×10^6 ES-2 cells/body and different doses of OPB-51602 were administered orally once daily for 14 days and then tumor volume was measured.

4.14. RT^2 profiler PCR array

H1975 cells were treated with 10 nM and 20 nM of OPB for 48 h prior to RNA extraction using QIAGEN RNeasy Mini Kit (QIAGEN, Germany) according to the manufacturer's instructions. cDNA synthesis was performed using QIAGEN RT^2 First Strand cDNA synthesis kit and qPCR measurement of customized RT^2 PCR plates using Applied Biosystem® 7500 Real-Time PCR System.

4.15. Study assessments

Safety evaluations occurred at baseline and weekly intervals for the duration of treatment, and within 15 days of last dosing. Evaluations included physical examination, electrocardiography, laboratory studies (hematology, clinical chemistries and urinalysis). The serial monitoring of serum lactate levels was introduced in cohort C, after preclinical data demonstrated lactate accumulation in OPB-51602-treated cells. AEs were graded according to the Common Terminology Criteria for Adverse Events (version 4.0). Radiological assessments by computerized tomography +/- radioisotope bone scans were performed during screening and following the first cycle, and after every 2 cycles thereafter. In the expansion cohorts, ^{18}F-fluorodeoxyglucose-positron-emission tomography (FDG-PET)/CT scan was used for baseline and post-cycle 1 assessment. Lesions were evaluated using Response Evaluation Criteria in Solid Tumors (RECIST) v1.1 and EORTC PET response criteria.

4.16. Study approval

All studies were reviewed and approved by the IRBs of the NMRC; the National University Hospital and written informed consent was received from participants prior to inclusion in the study. All animals were handled in accordance with the standards of Laboratory Animal Care.

4.17. Statistical analysis

For all in vitro experiments, three independent experiments were conducted and p-values were calculated using two-tailed paired or unpaired student's *t*-test and two-way ANOVA using GraphPad Prism software (Prism 7.0). P-values < 0.05 were considered statistically significant and all P-values are mentioned in the figures and figure legends.

4.18. Clinical data methodology

Clinical information was extracted from two different clinical trials of OPB-51602 as described in earlier publication [13]. This single-arm, open-label phase I trial was conducted in 3 cohorts; a dose-escalation, followed by two expansion cohorts evaluating intermittent and continuous dosing of the dose lower than the maximum-tolerated-dose, respectively. The study enrolled the patients with advanced, treatment-refractory solid tumors; subjects were treated until disease progression or intolerable toxicities. Radiological assessments by computerized tomography and radioisotope bone scans (where indicated), were performed during screening and following the first cycle, and after every 2 cycles thereafter. In the expansion cohorts, ^{18}F-fluorodeoxyglucose-positron-emission tomography (FDG-PET)/CT scan was used for baseline and post-cycle 1 assessment. Lesions were evaluated using Response Evaluation Criteria in Solid Tumors (RECIST) v1.1 and EORTC PET response criteria.

Authors' contributions

SP, GBC, AW, JT, JQE and JH wrote the manuscript. JH, JQE and JT designed the experiments. Clinical and animal data was provided by AW, NO and TT. JH, JQE, JT, AW and KLR performed experiments and interpreted data. JH, JQE, AW, JT, JQ and MVC provided technical and material support. This study was supervised by SP and GBC.

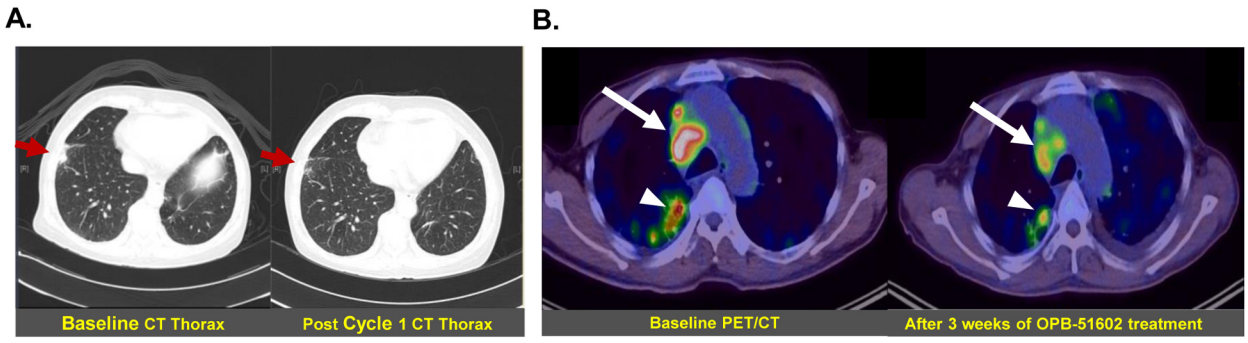

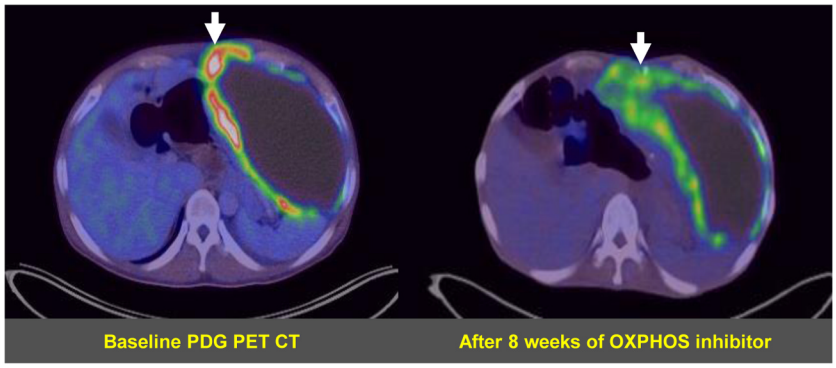

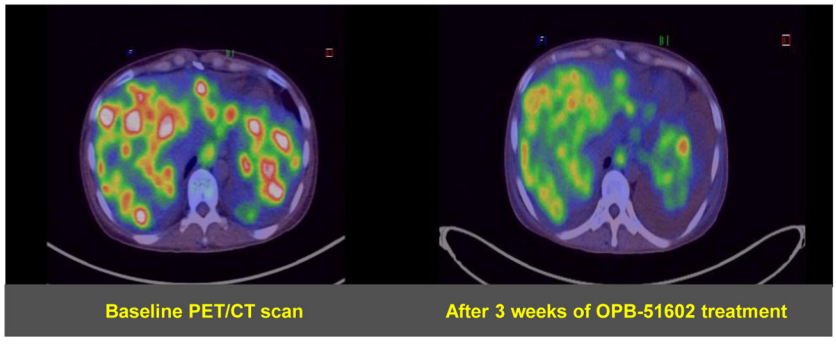

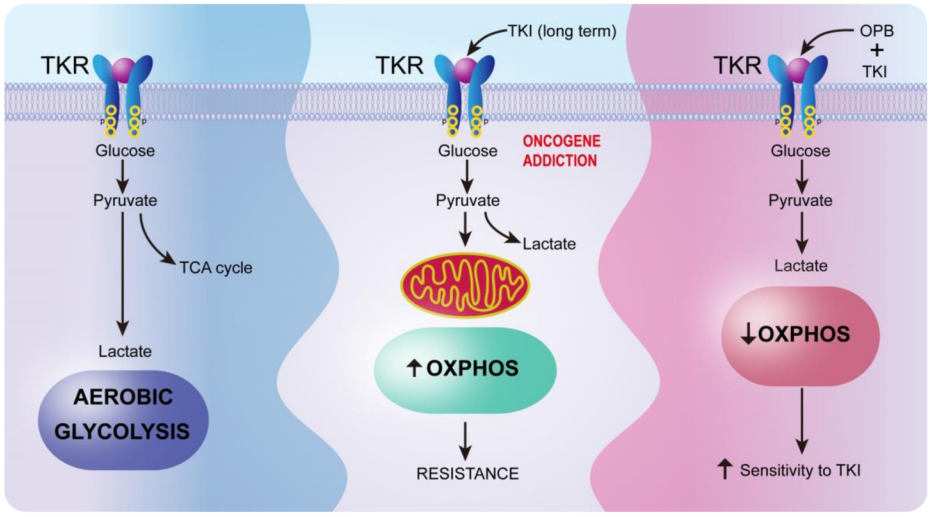

(caption on next page)

Fig. 6. ***Patients harboring heavily pre-treated or metastatic cancers respond positively to OPB-51602 treatment.*** **(A)** CT scan shows a right-sided pleural nodule (arrow, left panel) in a lady with EGFR TKI-resistant NSCLC. After 1 cycle of OPB-51602 treatment, the pleural nodule has shown significant reduction in size (right panel). **(B)** An ^{18}F-fluorodeoxyglucose–positron-emission tomographic (FDG–PET) scan showing FDG-avid right paratracheal lymph node (SUVmax 10.9; arrow, left panel) and a right lower lobe lung nodule (SUVmax 13.4; arrowhead, left panel) in a 61 year old man with non-small cell lung cancer (NSCLC). After 3 weeks of OPB-51602 treatment, there was significant reduction in metabolic activity of both lesions [SUVmax of the right paratracheal lymph node was 6.8 (arrow); SUVmax of the right lower lobe lung nodule was 8.3 (arrowhead), right panel]. **(C)** An FDG–PET scan showing an FDG-avid peritoneal nodule (SUVmax 18.8; arrow, left panel) in a 42 year old man with C-KIT mutation positive imatinib-refractory gastrointestinal stromal tumor (GIST). After 8 weeks of OXPHOS inhibitor treatment, there was significant reduction in SUVmax of the lesion to 11.3 (arrow, right panel). **(D)** An FDG–PET scan showing multiple FDG-avid liver metastases (SUVmax 13.6, arrow, left panel) in a young lady with heavily pre-treated NPC. After 3 weeks of OPB-51602 treatment, there was significant reduction in metabolic activity of the liver lesions (SUVmax 7.2, arrow, right panel). **(E)** Schematic representation of increased OXPHOS dependence of oncogene-addicted TKI-resistant tumors. Left panel shows tumor cells depend on aerobic glycolysis. Middle panel shows prolonged exposure to TKI results in metabolic reprogramming and switch to OXPHOS dependent bioenergetics, which drives the development of therapy resistance. Right panel shows pretreatment with OXPHOS inhibitor OPB-51602 target this vulnerability and restores sensitivity to TKI.

CRediT authorship contribution statement

Jayshree Hirpara: Conceptualization, Data curation, Formal analysis, Investigation, Methodology, Project administration, Writing - original draft, Writing - review & editing. **Jie Qing Eu:** Conceptualization, Data curation, Formal analysis, Investigation, Methodology, Project administration, Writing - original draft. **Joanna Kia Min Tan:** Conceptualization, Data curation, Formal analysis, Investigation, Methodology, Writing - original draft. **Andrea L. Wong:** Data curation, Formal analysis, Funding acquisition, Investigation, Methodology, Project administration, Resources, Writing - original draft. **Marie-Veronique Clement:** Formal analysis. **Li Ren Kong:** Data curation, Methodology, Project administration. **Naoto Ohi:** Methodology. **Takeshi Tsunoda:** Methodology. **Jianhua Qu:** Formal analysis, Project administration, Writing - review & editing. **Boon Cher Goh:** Conceptualization, Funding acquisition, Investigation, Resources, Supervision, Validation, Writing - original draft. **Shazib Pervaiz:** Conceptualization, Funding acquisition, Investigation, Resources, Supervision, Validation, Writing - original draft, Writing - review & editing.

Acknowledgments

Authors would like to thank Prof. Chng Wee Joo for providing Baf3 and its 3 mutant cell lines and Prof. Connolly for providing FLAG and HA tag STAT3 plasmid. Authors would also like to thank Dr. Koh Lie Yong Judice, Dr. Periyasamy Giridharan, Mr. Thangavelu Matan and Ms. Chan Jane Vin for the assistance with the HTS performed at Genome Institute of Singapore (GIS).

Funding support

(a) National Medical Research Council of Singapore (NMRC/CSA/021/2010), NMRC Bench to Bedside (BOB) to GBC, Ministry of Education (MOE) funded Experimental Therapeutics under CSI. (b) National University Health System Clinician Scientist Program Clinical Science Unit (CSU) to AW. (c) National Medical Research Council-Clinician Scientist Individual Research Grant (NMRC/CIRG/1433/2015) Grant to SP.

Disclosure of potential conflicts of interest

Apart from employment of two of the authors (TT and NO) as well as research funding of BCG and ALW by Otsuka Pharmaceutical Co. Ltd., all other authors express no conflicts of interest.

Appendix A. Supporting information

Supplementary data associated with this article can be found in the online version at doi:10.1016/j.redox.2018.101076

References

[1] L.A. Hindorff, E.M. Gillanders, T.A. Manolio, Genetic architecture of cancer and other complex diseases: lessons learned and future directions, Carcinogenesis 32 (2011) 945–954, https://doi.org/10.1093/carcin/bgr056.
[2] T.M. Ashton, W.G. McKenna, L.A. Kunz-Schughart, G.S. Higgins, Oxidative phosphorylation as an emerging target in cancer therapy, Clin. Cancer Res. (2018), https://doi.org/10.1158/1078-0432.CCR-17-3070.
[3] C. Jose, N. Bellance, R. Rossignol, Choosing between glycolysis and oxidative phosphorylation: a tumor's dilemma? Biochim. Biophys. Acta 1807 (2011) 552–561, https://doi.org/10.1016/j.bbabio.2010.10.012.
[4] G. Solaini, G. Sgarbi, A. Baracca, Oxidative phosphorylation in cancer cells, Biochim. Biophys. Acta 1807 (2011) 534–542, https://doi.org/10.1016/j.bbabio.2010.09.003.
[5] W. Luo, G.L. Semenza, Pyruvate kinase M2 regulates glucose metabolism by functioning as a coactivator for hypoxia-inducible factor 1 in cancer cells, Oncotarget 2 (2011) 551–556, https://doi.org/10.18632/oncotarget.299.
[6] H. Xie, M.C. Simon, Oxygen availability and metabolic reprogramming in cancer, J. Biol. Chem. 292 (2017) 16825–16832, https://doi.org/10.1074/jbc.R117.799973.
[7] L. Yu, et al., Modeling the genetic regulation of cancer metabolism: interplay between glycolysis and oxidative phosphorylation, Cancer Res. 77 (2017) 1564–1574, https://doi.org/10.1158/0008-5472.CAN-16-2074.
[8] A. Morandi, S. Indraccolo, Linking metabolic reprogramming to therapy resistance in cancer, Biochim. Biophys. Acta 1868 (2017) 1–6, https://doi.org/10.1016/j.bbcan.2016.12.004.
[9] H.J. Lee, et al., Drug resistance via feedback activation of Stat3 in oncogene-addicted cancer cells, Cancer Cell 26 (2014) 207–221, https://doi.org/10.1016/j.ccr.2014.05.019.
[10] C.M. Della Corte, M. Fasano, F. Papaccio, F. Ciardiello, F. Morgillo, Role of HGF-MET signaling in primary and acquired resistance to targeted therapies in cancer, Biomedicines 2 (2014) 345–358, https://doi.org/10.3390/biomedicines2040345.
[11] S.M. Kim, et al., Activation of the Met kinase confers acquired drug resistance in FGFR-targeted lung cancer therapy, Oncogenesis 5 (2016) e241, https://doi.org/10.1038/oncsis.2016.48.
[12] S.M. Leto, L. Trusolino, Primary and acquired resistance to EGFR-targeted therapies in colorectal cancer: impact on future treatment strategies, J. Mol. Med. 92 (2014) 709–722, https://doi.org/10.1007/s00109-014-1161-2.
[13] A.L. Wong, et al., Phase I and biomarker study of OPB-51602, a novel signal transducer and activator of transcription (STAT) 3 inhibitor, in patients with refractory solid malignancies, Ann. Oncol. 26 (2015) 998–1005, https://doi.org/10.1093/annonc/mdv026.
[14] D. Genini, et al., Mitochondrial dysfunction induced by a SH2 domain-targeting STAT3 inhibitor leads to metabolic synthetic lethality in cancer cells, Proc. Natl. Acad. Sci. USA 114 (2017) E4924–E4933, https://doi.org/10.1073/pnas.1615730114.
[15] X. Zhang, et al., A novel inhibitor of STAT3 homodimerization selectively suppresses STAT3 activity and malignant transformation, Cancer Res. 73 (2013) 1922–1933, https://doi.org/10.1158/0008-5472.CAN-12-3175.
[16] M. Barbi de Moura, et al., Mitochondrial respiration – an important therapeutic target in melanoma, PLoS One 7 (2012) e40690, https://doi.org/10.1371/journal.pone.0040690.
[17] T.M. Ashton, W.G. McKenna, L.A. Kunz-Schughart, G.S. Higgins, Oxidative phosphorylation as an emerging target in cancer therapy, Clin. Cancer Res. 24 (2018) 2482–2490, https://doi.org/10.1158/1078-0432.CCR-17-3070.
[18] M.D. Brand, D.G. Nicholls, Assessing mitochondrial dysfunction in cells, Biochem. J. 435 (2011) 297–312, https://doi.org/10.1042/BJ20110162.
[19] L.S. Pike Winer, M. Wu, Rapid analysis of glycolytic and oxidative substrate flux of cancer cells in a microplate, PLoS One 9 (2014) e109916, https://doi.org/10.1371/journal.pone.0109916.
[20] E.M. Kuntz, et al., Targeting mitochondrial oxidative phosphorylation eradicates therapy-resistant chronic myeloid leukemia stem cells, Nat. Med. 23 (2017) 1234–1240, https://doi.org/10.1038/nm.4399.
[21] P. Sancho, et al., MYC/PGC-1alpha balance determines the metabolic phenotype and plasticity of pancreatic cancer stem cells, Cell Metab. 22 (2015) 590–605, https://doi.org/10.1016/j.cmet.2015.08.015.
[22] F. Obrist, et al., Metabolic vulnerability of cisplatin-resistant cancers, EMBO J. 37 (2018), https://doi.org/10.15252/embj.201798597.

[23] K.M. Lee, et al., MYC and MCL1 cooperatively promote chemotherapy-resistant breast cancer stem cells via regulation of mitochondrial oxidative phosphorylation (e637), Cell Metab. 26 (2017) 633–647, https://doi.org/10.1016/j.cmet.2017.09.009.
[24] E. Batlle, H. Clevers, Cancer stem cells revisited, Nat. Med. 23 (2017) 1124–1134, https://doi.org/10.1038/nm.4409.
[25] K. Ito, T. Suda, Metabolic requirements for the maintenance of self-renewing stem cells, Nat. Rev. Mol. Cell Biol. 15 (2014) 243–256, https://doi.org/10.1038/nrm3772.
[26] L. Ippolito, et al., Metabolic shift toward oxidative phosphorylation in docetaxel resistant prostate cancer cells, Oncotarget 7 (2016) 61890–61904, https://doi.org/10.18632/oncotarget.11301.
[27] G. Kroemer, J. Pouyssegur, Tumor cell metabolism: cancer's Achilles' heel, Cancer Cell 13 (2008) 472–482, https://doi.org/10.1016/j.ccr.2008.05.005.
[28] J. Kasznicki, A. Sliwinska, J. Drzewoski, Metformin in cancer prevention and therapy, Ann. Transl. Med. 2 (2014) 57, https://doi.org/10.3978/j.issn.2305-5839.2014.06.01.
[29] M.Y. El-Mir, et al., Dimethylbiguanide inhibits cell respiration via an indirect effect targeted on the respiratory chain complex I, J. Biol. Chem. 275 (2000) 223–228.
[30] M.N. Pollak, Investigating metformin for cancer prevention and treatment: the end of the beginning, Cancer Discov. 2 (2012) 778–790, https://doi.org/10.1158/2159-8290.CD-12-0263.
[31] M. Pollak, Targeting oxidative phosphorylation: why, when, and how, Cancer Cell 23 (2013) 263–264, https://doi.org/10.1016/j.ccr.2013.02.015.